Numerical Study of Microwave Scattering in Breast Tissue via Coupled Dielectric and Elastic Contrasts

Min Zhao, *Student Member, IEEE*, Jacob D. Shea, *Student Member, IEEE*, Susan C. Hagness, *Senior Member, IEEE*, Daniel W. van der Weide, *Senior Member, IEEE*, Barry D. Van Veen, *Fellow, IEEE*, and Tomy Varghese, *Senior Member, IEEE*

***Abstract*—A computational investigation of microwave scattering in mechanically (or acoustically) excited breast tissue is conducted to explore the feasibility of combining dielectric and elastic properties contrasts to enhance breast cancer detection. The mechanical excitation induces tissue-dependent displacements in the heterogeneous breast interior, which modulate the scattered microwave signals. Sheet boundary conditions are implemented using the finite-difference time-domain (FDTD) method to efficiently compute the Doppler component of the scattered microwave signals. Simulation results for a 2D numerical phantom testbed demonstrate increased microwave scattering contrast between malignant and normal fibroglandular inclusions when elastic properties are exploited.**

***Index Terms*—Biomechanics, breast cancer detection, dielectric properties, elastic properties, finite-difference time-domain (FDTD), finite element method (FEM), microwave imaging, scattering.**

I. Introduction

THE potential use of microwaves for detecting breast tumors has received significant attention in recent years. The physical basis for the three emerging classes of active microwave techniques is tissue-dependent microwave scattering and selective absorption in the breast. In microwave radar [1], [2] and microwave tomography [3], [4] systems, low-power microwave signals are transmitted into the breast using an array of antennas which in turn measure the scattered microwave signals. In microwave-induced thermoacoustic approaches [5], [6], microwave signals are transmitted into the breast to slightly heat higher-conductivity tissue and ultrasound transducers measure the pressure waves generated by the consequent tissue expansion. All of these techniques attempt to exploit differences in the microwave-frequency dielectric properties of malignant and normal breast tissues—the subject of a recently published large-scale dielectric spectroscopy study [7], [8].

Different types of tissue in the breast also exhibit contrasts in their elastic properties [9]. Namely, cancerous tissue is much stiffer than both adipose tissue and normal fibroglandular tissue. This contrast serves as the physical basis for breast imaging via elastography [10]–[12].

In this letter, we propose a hybrid sensing approach for breast cancer detection that uses microwave and acoustic or mechanical excitations to exploit contrasts in both the dielectric and elastic properties of malignant and normal breast tissue. The objective of this hybrid method is to enhance the electromagnetic scattering contrast for use in microwave tumor detection or diagnosis. While acousto-optics techniques that couple acoustic modulation with laser light scattering have been previously explored [13]–[16], the scattering mechanisms and the electromagnetic properties of interest are quite different at microwave frequencies. Section II describes the concept using a simple 1D illustration. Section III describes the 2D simulation approach we use to investigate microwave scattering from malignant and normal breast tissue targets undergoing mechanical deformation. Section IV presents the 2D numerical phantom testbed used to obtain the results given in Section V.

II. Hybrid Modality Concept

The proposed hybrid approach applies low-frequency acoustic or mechanical excitation to induce tissue-dependent displacements within the heterogeneous breast while low power microwave signals are transmitted into breast and the scattered microwave signals are measured using an antenna array. The induced tissue deformations modulate the scattered microwave signals detected by the receiver. The effect of tissue displacement on microwave backscatter can be easily illustrated with a simple 1D example. We assume that the surface of a lossless dielectric half-space is displaced sinusoidally at frequency ω_m and with peak displacement A_m. The half-space is illuminated by an electromagnetic plane wave of amplitude E_0 and frequency ω_0. The phase of the scattered field $E_s(t)$ is modulated by the moving boundary, resulting in a scattered field that can be expressed as follows in terms of discrete Doppler spectra [17]:

$$E_s(t) = \Gamma E_0 \sum_{n=-\infty}^{+\infty} J_n\left(\frac{4\pi A_m}{\lambda_0}\right) \cos\left((\omega_0 + n\omega_m)t\right) \quad (1)$$

Here Γ is the reflection coefficient at the interface in the absence of motion, J_n is the n^{th} order Bessel function, and λ_0 is the wavelength of the plane wave in the incident medium, which is also assumed to be lossless in this illustrative example. Note that the signal depends on both dielectric properties contrast through Γ and elastic properties contrast through A_m.

Manuscript received January 4, 2008; revised February 14, 2008. This work was supported by the Department of Defense Breast Cancer Imaging Research Program under Grant W81XWH-04-1-0356 and the National Institutes of Health under Grant R01 CA112398 awarded by the National Cancer Institute.

M. Zhao, J. D. Shea, S. C. Hagness, D. W. van der Weide and B. D. Van Veen are with the Department of Electrical and Computer Engineering, University of Wisconsin, Madison, WI 53706 USA (e-mail: minz@cae.wisc.edu; shea@cae.wisc.edu; hagness@engr.wisc.edu; danvdw@engr.wisc.edu; vanveen@engr.wisc.edu).

T. Varghese is with the Department of Medical Physics, University of Wisconsin, Madison, WI 53706 USA (e-mail: tvarghese@facstaff.wisc.edu).

Digital Object Identifier 10.1109/LAWP.2008.920752

This simple 1D example offers a conceptual illustration of the potential role of the hybrid approach for enhancing the sensitivity of microwave breast cancer detection. The recent dielectric characterization study by Lazebnik *et al.* [7], [8] indicates that a large dielectric contrast exists between malignant tissue and normal adipose-dominated tissue, while the contrast between malignant and normal fibroglanduar tissue is much smaller. The introduction of a Doppler component that depends on elastic properties enhances the information content of the microwave scattered signal and may lead to better discrimination between cancerous tumors and normal fibroglandular masses.

III. Numerical Simulation Methods

This type of multiphysics problem involves two distinct time scales: the shorter electromagnetic time scale associated with steady-state conditions at microwave frequencies (∼GHz) and the longer mechanical time scale associated with low-frequency acoustic or mechanical excitations (kHz or less). A common approach to analyzing or simulating such problems involves the use of the quasi-stationary (QS) approximation [18], [19] wherein the scattered field is calculated as if the scattering object were stationary at any instance in time. Our approach for modeling this multi-physics problem with the QS approximation involves two types of numerical simulations. First, a mechanical simulation, based on a finite element method (FEM) solution of a plain-strain partial differential equation, is conducted to compute tissue deformation under mechanical excitation. Next, electromagnetic simulations, based on a finite-difference time-domain (FDTD) solution of Maxwell's equations, model the microwave interactions with stationary snapshots of the tissue.

Clinically feasible mechanical displacements of breast tissue (on the order of mm or less) are much smaller than the microwave wavelength in the medium (normal fatty or normal glandular tissue) that surrounds the scattering object (normal glandular or malignant glandular tissue). The challenges of spatially resolving the small tissue displacements in the FDTD grid and accurately calculating the small Doppler component of the scattered field can be overcome by modeling the vibrating object as a stationary object with time-varying sheet boundary conditions (SBCs) [19], [20]. The total scattered field is decomposed into the unperturbed field scattered by the stationary object and a Doppler field perturbation, $\overrightarrow{E_d}$, associated with the vibration of the object. First, an FDTD simulation is conducted to compute the scattered fields from the unperturbed object illuminated by the incident electromagnetic wave. Next, the equivalent surface currents for the SBC are calculated using the unperturbed field solutions and peak boundary displacements computed from the mechanical simulation. Detailed expressions for the currents are given in [20] and are valid for small displacements relative to the microwave wavelength—a regime that is indeed consistent with our proposed application. Finally, a second FDTD simulation is conducted to compute $\overrightarrow{E_d}$ using equivalent surface currents on the stationary object as the only sources.

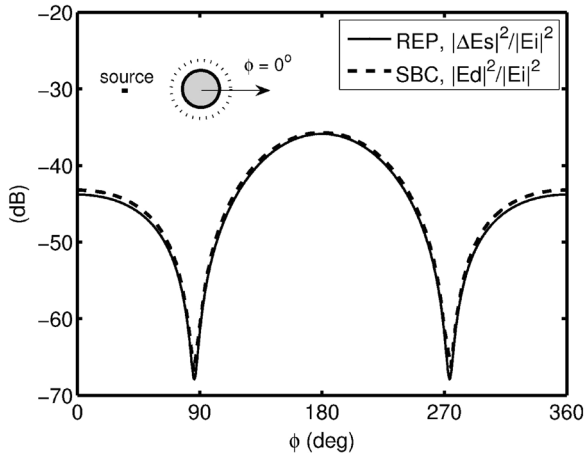

Fig. 1. Comparison of the amplitudes of the normalized Doppler component computed via FDTD-SBC (dashed line) and the normalized difference between stationary scattered field solutions computed via FDTD-REP (solid line). The 2D scattering object is a deforming 4-mm-diameter circular cylinder undergoing a peak radial displacement of 0.45 mm.

We validate our implementation of the FDTD-SBC method for the 2D TM_z case by comparing its results with those generated by a brute-force method in which the boundary of the scattering object is repositioned. This benchmark approach, which we denote as FDTD-REP, requires two FDTD simulations in which the scattered fields are computed for the same microwave illumination but different stationary scattering objects: an unperturbed object and the same object under peak applied strain. The FDTD-REP solution, $\overrightarrow{\Delta E_s}$, is calculated as the difference between the two sets of scattered fields. It can be shown analytically for the simple 1D problem described in the previous section that the amplitude of $\overrightarrow{\Delta E_s}$ is an excellent approximation to the amplitude of the Doppler component, $\overrightarrow{E_d}$, of the actual scattered field induced by the vibrations, provided that $A_m \ll \lambda_0$. Thus the use of the amplitude of the FDTD-REP solution as a benchmark is appropriate for the small deformations considered here.

The scattering object in our 2D TM_z validation study is a 4-mm-diameter cylinder ($\epsilon_r = 50$, $\sigma_s = 4.910\,\mathrm{S/m}$) in a homogeneous background material ($\epsilon_r = 44$, $\sigma_s = 4.162\,\mathrm{S/m}$). The radius of the inclusion is assumed to vary sinusoidally in time and uniformly across azimuthal angle, with a peak radial deformation of 0.45 mm. The incident wave is launched by an electric current line source 7.5 cm away from the inclusion center. We select electric field observation points 4 cm away from the inclusion center. Fig. 1 shows the normalized amplitude of $\overrightarrow{E_d}$ and $\overrightarrow{\Delta E_s}$ computed at 5 GHz using FDTD-SBC and FDTD-REP, respectively. The excellent agreement between these two set of results demonstrates the accuracy of our FDTD-SBC implementation.

IV. Numerical Testbed

Our 2D numerical phantom testbed is designed to simulate a scenario that is challenging for microwave detection schemes that are based solely on dielectric contrast. That is, we investigate microwave scattering from a cylindrical inclusion of malignant tissue ($\epsilon_r = 50$, $\sigma_s = 4.91\,\mathrm{S/m}$ at 5 GHz) surrounded by

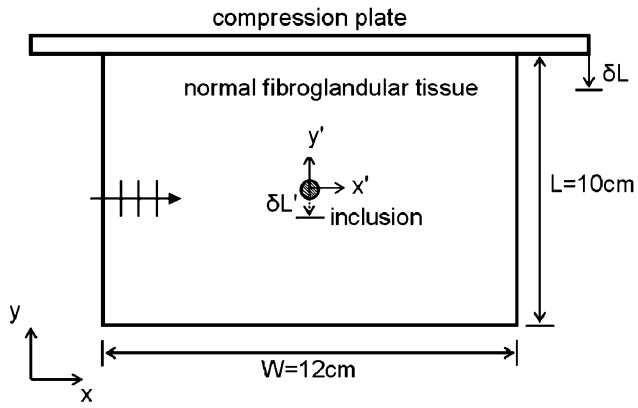

Fig. 2. Phantom configuration for the hybrid simulations, with axis of cylindrical inclusion into the page.

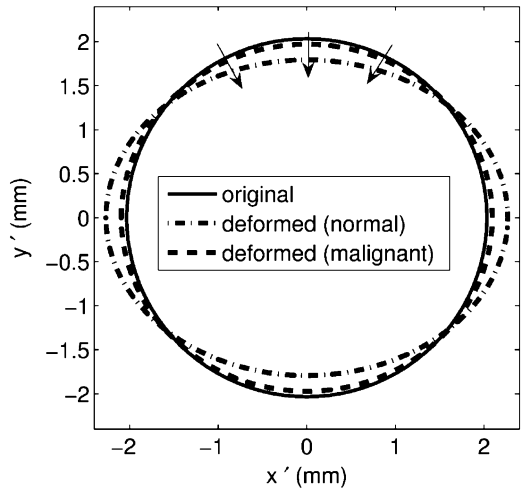

Fig. 3. Deformed inclusion boundaries, under a 10% peak applied strain. Peak deformation of boundary point (0, 2) is 0.24 mm for the normal fibroglandular inclusion and 0.07 mm for the malignant tumor inclusion.

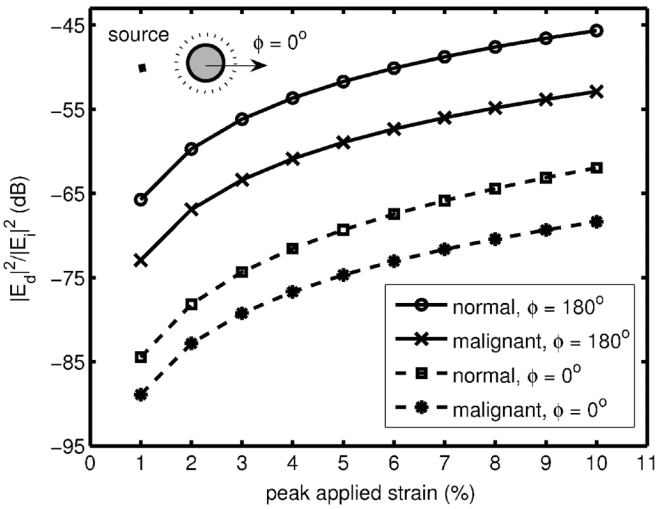

Fig. 4. Computed Doppler components in the backward ($\phi = 180°$) and forward ($\phi = 0°$) scattered fields under different peak applied strains, for malignant and normal fibroglandular scatterers.

normal tissue that has significant fibroglandular content ($\epsilon_r = 35$, $\sigma_s = 3.09\ \mathrm{S/m}$). For reference, we also consider scattering from a fibroglandular mass ($\epsilon_r = 44$, $\sigma_s = 4.16\ \mathrm{S/m}$) surrounded by the same normal tissue environment. In both cases, the scattering object (tumor or fibroglandular inclusion) is a 4-mm-diameter circular cylinder. The dielectric properties values assigned to the different tissues are derived from the data reported in [7], [8]. While the tumor detection scenario described above involves a relatively small dielectric contrast between the scattering object and the surrounding medium, there is a large elastic properties contrast. Using the measured data with 2% applied strains reported in [9], we assign the tumor a Young's modulus of $\mathrm{E} = 12\ \mathrm{Kpa}$, while the surrounding normal tissue is modeled with the Young's modulus reported for fibroglandular tissue ($\mathrm{E} = 1.8\ \mathrm{Kpa}$). For the reference scenario, we assume $\mathrm{E} = 1.8\ \mathrm{Kpa}$ throughout the entire phantom (both the fibroglandular inclusion as well as the surrounding normal tissue). We also assume a linear stress-strain relationship in the simulated breast tissues under small applied strain levels of 1–10%. All tissue types are modeled using the same Poisson's ratio ($\nu = 0.495$).

In the mechanical simulation, the inclusion is embedded 5 cm below the upper surface of the 12 cm × 10 cm domain, as shown in Fig. 2. A mechanical compression plate is placed on the upper surface to apply an excitation with a peak strain of δL. In simulation, we have applied peak strains from 1 mm to 10 mm (i.e., $\delta L/L = 1{-}10\%$). We use the Comsol v3.3 structural mechanics module to conduct this FEM-based simulation and obtain tissue-dependent deformations. In addition, in order to isolate the elasticity-dependent inclusion deformations only, we subtract the vertical body movement of the inclusion center $\delta L'$ from the total simulated displacements. This calibrated deformation data from the mechanical simulation is imported into the FDTD-SBC electromagnetic simulation. The FDTD grid sampling density is $N = \lambda_0/\Delta x = 40$, where λ_0 is the wavelength at 5 GHz in the surrounding normal tissue. The incident wave is launched by an electric current line source 7.5 cm away from the scatterer center. In this feasibility study, complicating effects due to scattering from the breast surface are avoided by filling the entire electromagnetic computational domain (aside from the inclusion region) with the normal breast tissue background medium. We select electric field observation points 4 cm away from the scatterer center.

V. Results

The mechanical simulation results, reported in Fig. 3, show the deformation of inclusion boundaries for the malignant tumor or normal fibroglandular inclusion, when we apply a 10% peak strain. The normal fibroglandular tissue inclusion experiences more than three times the boundary deformation of the malignant mass. The peak deformation of the top boundary of the inclusion (coordinates $x' = 0$, $y' = 2\ \mathrm{mm}$) is 0.24 mm for the normal fibroglandular inclusion and 0.07 mm for the malignant tumor.

The subsequent electromagnetic simulation results, summarized in Fig. 4, show the Doppler component in the backward ($\phi = 180°$) and forward ($\phi = 0°$) scattered fields for the

deforming scatterers as a function of the peak applied strain. We observe stronger Doppler scattering from the deforming normal fibroglandular inclusion than from the deforming malignant tumor. The harmonic backscattered signal from the normal fibroglandular inclusion is 8 dB higher than that from the malignant tumor. In comparison, the backscattered signal from the unperturbed normal fibroglandular mass (in which case only the dielectric properties play a role) is 3.5 dB lower than that from the unperturbed malignant tumor. Hence, these results show the promise of using this hybrid modality to enhance the overall microwave scattering contrast for the purpose of distinguishing cancerous tumors from normal fibroglandular tissue in the breast.

VI. Conclusion

Our 2D computational study of a hybrid modality that exploits both dielectric and elastic tissue property-contrasts reveals the potential for enhancing overall microwave scattering contrast between normal and malignant fibroglandular tissues. This is an important finding in light of the recent insights gained from the large-scale dielectric spectroscopy study reported by Lazebnik *et al.* [7], [8]. We will extend this study to 3D and work with a more realistic breast model in the future.

Acknowledgment

The authors would like to thank Prof. R. H. Blick at the University of Wisconsin for allowing them to use his group's Comsol software.

References

[1] X. Li, E. J. Bond, B. D. Van Veen, and S. C. Hagness, "An overview of ultrawideband microwave imaging for early-stage breast cancer detection," *IEEE Antennas Propag. Mag.*, vol. 47, pp. 19–34, Feb. 2005.

[2] J. M. Sill and E. C. Fear, "Tissue sensing adaptive radar for breast cancer detection—Experimental investigation of simple tumor models," *IEEE Trans. Microw. Theory Tech*, vol. 53, no. 11, pp. 3312–3319, Nov. 2005.

[3] P. M. Meaney, M. W. Fanning, T. Raynolds, C. J. Fox, Q. Fang, C. A. Kogel, S. P. Poplack, and K. D. Paulsen, "Initial clinical experience with microwave breast imaging in women with normal mammography," *Academy Radiology*, vol. 14, pp. 207–218, Feb. 2007.

[4] D. W. Winters, E. J. Bond, B. D. Van Veen, and S. C. Hagness, "Estimation of the frequency-dependent average dielectric properties of breast tissue using a time-domain inverse scattering technique," *IEEE Trans. Antennas Propag.*, vol. 54, no. 11, pp. 3517–3528, Nov. 2006.

[5] G. Ku, B. D. Fornage, X. Jin, M. H. Xu, K. K. Hunt, and L. V. Wang, "Thermoacoustic and photoacoustic tomography of thick biological tissues toward breast imaging," *Tech. Cancer Res. Treatment*, vol. 4, pp. 559–565, Oct. 2005.

[6] R. A. Kruger, K. D. Miller, H. E. Reynolds, W. L. Kiser, Jr., D. R. Reinecke, and G. A. Kruger, "Breast cancer in vivo: Contrast enhancement with thermoacoustic CT at 434 MHz—Feasibility study," *Radiology*, no. 216, pp. 279–283, 2000.

[7] M. Lazebnik, L. McCartney, D. Popovic, C. B. Watkins, M. J. Lindstrom, J. Harter, S. Sewall, A. Magliocco, J. H. Booske, M. Okoniewski, and S. C. Hagness, "A large-scale study of the ultrawideband microwave dielectric properties of normal breast tissue obtained from reduction surgeries," *Phys. Med. Biol.*, vol. 52, pp. 2637–2656, May 2007.

[8] M. Lazebnik, D. Popovic, L. McCartney, C. B. Watkins, M. J. Lindstrom, J. Harter, S. Sewall, T. Ogilvie, A. Magliocco, T. M. Breslin, W. Temple, D. Mew, J. H. Booske, M. Okoniewski, and S. C. Hagness, "A large-scale study of the ultrawideband microwave dielectric properties of normal, benign and malignant breast tissues obtained from cancer surgeries," *Phys. Med. Biol.*, vol. 52, pp. 6093–6115, Oct. 2007.

[9] A. Samani, J. Bishop, C. Luginbuhl, and D. B. Plewes, "Measuring the elastic modulus of ex vivo small tissue samples," *Phys. Med. Biol.*, vol. 48, pp. 2183–2198, Jul. 2003.

[10] J. C. Bamber, P. E. Barbone, and N. L. Bush, "Progress in freehand elastography of the breast," *IEICE Trans. Info. Sys.*, vol. E85D, pp. 5–14, Jan. 2002.

[11] J. Ophir, S. K. Alam, B. Garra, F. Kallel, E. Konofagou, T. Krouskop, and T. Varghese, "Elastography: Ultrasound estimation and imaging of the elastic properties of tissues," in *Proc. Institution Mechanical Eng.*, 1999, vol. 213(H3), pp. 203–233.

[12] R. Sinkus, M. Tanter, T. Xydeas, S. Catheline, J. Bercoff, and M. Fink, "Viscoelastic shear properties of in vivo breast lesions measured by MR elastography," *Magn. Reson Imaging*, vol. 23, pp. 159–165, Feb. 2005.

[13] H. T. Banks, M. W. Buksas, and T. Lin, *Electromagnetic Material Interrogation Using Conductive Interfaces and Acoustic Wavefronts*. Philadelphia, PA: Society for Industrial and Applied Mathematics, 2000.

[14] L. Wand, S. L. Jacques, and X. Zhao, "Continuous-wave ultrasonic modulation of scattered laser light to image objects in turbid media," *Opt. Lett.*, vol. 20, pp. 629–631, 1995.

[15] M. Kempe, M. Larionov, D. Zaslavsky, and A. Z. Genack, "Acoustooptic tomography with multiply scattered light," *J. Opt. Soc. Am. A*, vol. 14, pp. 1151–1158, May 1997.

[16] L. Wang and X. Zhao, "Ultrasound-modulated optical tomography of absorbing objects buried in dense tissue simulating turbid media," *Appl. Opt.*, vol. 36, pp. 7277–7282, Oct. 1997.

[17] S. Haykin, *Communication Systems*. New York: Wiley, 2001.

[18] J. Van Bladel, "Electromagnetic fields in the presence of rotating bodies," *Proc. IEEE*, vol. 64, pp. 301–318, March 1976.

[19] D. E. Lawrence and K. Sarabandi, "Electromagnetic scattering from vibrating penetrable objects using a general class of time-varying sheet boundary conditions," *IEEE Trans. Antennas Propag.*, vol. 54, no. 7, pp. 2054–2061, Jul. 2006.

[20] A. M. Buerkle and K. Sarabandi, "Analysis of acousto-electromagnetic wave interaction using sheet boundary conditions and the finite-difference time-domain method," *IEEE Trans. Antennas Propag.*, vol. 55, no. 7, pp. 1991–1998, Jul. 2007.